I.J. Image, Graphics and Signal Processing, **2023, 6, 41-53**
Published Online on December 8, 2023 by MECS Press (http://www.mecs-press.org/)
DOI: 10.5815/ijigsp.2023.06.04

Analytical and Computer Polarization-Correlation Processing of Brest Tumors' Laser Fields for Cancer Detection

Yuriy Ushenko*
Computer Science Department, Yuriy Fedcovitch Chernivtsi National University, Chernivtsi, Ukraine, 58002
E-mail: y.ushenko@chnu.edu.ua
ORCID ID: https://orcid.org/0000-0003-1767-1882
*Corresponding Author

Valentina Dvorzhak
Computer Science Department, Yuriy Fedcovitch Chernivtsi National University, Chernivtsi, Ukraine, 58002
E-mail: v.dvorzhak@chnu.edu.ua
ORCID ID: https://orcid.org/0000-0003-4772-6688

Oleksandr Dubolazov
Optics and Publishing Department, Yuriy Fedcovitch Chernivtsi National University, Chernivtsi, Ukraine, 58002
E-mail: a.dubolazov@chnu.edu.ua
ORCID ID: https://orcid.org/0000-0003-1051-2811

Oleksandr Ushenko
Optics and Publishing Department, Yuriy Fedcovitch Chernivtsi National University, Chernivtsi, Ukraine, 58002
E-mail: o.ushenko@chnu.edu.ua
ORCID ID: https://orcid.org/0000-0001-7015-7423

Ivan Mikirin
Optics and Publishing Department, Yuriy Fedcovitch Chernivtsi National University, Chernivtsi, Ukraine, 58002
E-mail: mikirin.ivan@chnu.edu.ua
ORCID ID: https://orcid.org/0000-0002-7319-6636

Zhengbing Hu
School of Computer Science, Hubei University of Technology, Wuhan, China
E-mail: drzbhu@gmail.com
ORCID ID: https://orcid.org/0000-0002-6140-3351

Received: 17 July, 2023; Revised: 21 August, 2023; Accepted: 23 September, 2023; Published: 08 December, 2023

Abstract: A new local-topological approach to describe the spatial and angular distributions of polarization parameters of multiply scattered optically anisotropic biological layers of laser fields is considered. A new analytical parameter to describe the local polarization structure of a set of points of coherent object fields, the degree of local depolarization (DLD), is introduced for the first time. The experimental scheme and the technique of measuring coordinate distributions (maps) of DLD The new method of local polarimetry was experimentally tested on histological specimens of biopsy sections of operatively extracted breast tumors. The measured DLD maps were processed using statistical, autocorrelation and scale-sampling approaches. Markers for differential diagnosis of benign (fibroadenoma) and malignant (sarcoma) breast tumors were defined.

Index Terms: Local degree of depolarization, coherence, scattering, biological tissue, optical anisotropy, cancer.

1. Introduction

Optical analysis of tissue types offers distinct advantages, being non-destructive, requiring limited sample preparation, and being cheap and fast. Analysis of the polarization properties- known as polarimetric diagnostics- of different tissues holds great promise. Polarimetric diagnostics of optically anisotropic biological tissues are undergoing active development in biomedical optics. Several key strands of investigation have emerged, including Mueller matrix mapping using various approximations, computer proceedings and optically devises. At the same time, the listed "one-point" methods have a number of disadvantages - the azimuthal dependence of the structure of polarization and Muller-matrix maps. In addition, the sensitivity and accuracy of diagnostics of the polycrystalline structure of biological layers decrease with an increase in the level of the depolarized background.

All this complicates the clinical application of methods and means of "one-point" 2D polarization mapping in serial measurements of biological products. Such limitations can be overcome by developing a new azimuthally invariant "two-point" methods Stokes-correlometry of polarization-inhomogeneous object.

Our work is devoted to developing a new polarization-correlation approach to the description of laser fields scattered by diffuse biological layers in order to determine the possibility of using a new analytical parameter for the description of the laser fields multiply scattered by diffuse biological layers. On this basis, the possibility of cancer diagnosis by mapping the local depolarization degree distributions of microscopic images of histological sections of breast tumors biopsies was investigated.

2. Brief Theory

The most common approach in the analysis of light scattering processes of laser radiation by biological layers is statistical processing of obtained distributions of experimental data [1,2].

The development of this approach was a new direction of optical diagnostics - laser polarimetry of optically thin layers of biological tissues and liquids [4 - 6]. Within its framework, diagnostically relevant relationships between a set of statistical, autocorrelation and scale-self parameters and changes in birefringence of biological layers were found.

Most biological objects are highly scattering structures that depolarize laser radiation. As a result, the diagnostic efficiency of laser polarimetry techniques is significantly reduced [7-10]. On the other hand, when coherent laser radiation is scattered, a speckle field is formed with a 100% degree of local polarization [11]. Therefore, the development of new correlation approaches [12 - 20] to the description of the mechanisms of the formation of depolarization multiply scattered by layers of optically thick BT laser radiation is of current interest in various technical tasks including machine learning systems [21-25].

3. Investigation Methodology

The research methodology involves the implementation of a set of sequential and complementary analytical steps. In the first stage, the Jones matrix description of optical anisotropy of histological sections of benign and malignant breast tumors is proposed for the analytical determination and physical justification of diagnostic relevant relationships between the local degree of depolarization phase (DLD). Based on the obtained analytical relationships, a technique for the experimental measurement of coordinate distributions of DLD phase (polarization-correlation maps) is developed using a traditional imaging Stokes polarimeter setup. For the set of measured polarization-correlation maps within representative samples, statistical, correlational, and fractal parameters are computed. As a result, markers that are most sensitive to changes in birefringence of benign and malignant tumor samples are identified.

4. Brief Theory and Basic Analytical Relationships

The present study aims to obtain a set of analytical relationships describing the correlations between parameters of optical anisotropy in biological samples and a new polarization-correlation parameter, the degree of coherence modulus. These derived relationships serve as the foundation for developing an experimental methodology to measure polarization-correlation maps and perform a physical analysis of the obtained data. The ultimate goal is to identify a set of new markers in breast cancer oncology.

We based our theoretical consideration on the following optical model representations:

- We describe the optical properties of the histological slice layer of a breast tumor biopsy by two components, surface or optically isotropic and bulk optically anisotropic.
- Polarization manifestations of birefringence of the volumetric layer of a biological preparation can be described by the Jones matrix operator of the following form.

$$\{B\}=\begin{bmatrix} b_{11} & b_{12} \\ b_{21} & b_{22} \end{bmatrix}=\begin{bmatrix} cos^2\,\theta\,(r)+sin^2\,\theta\,(r)\,exp\big(-i\varphi(r)\big); & cos\,\theta\,(r)\,sin\,\theta\,(r)\big(1-exp\big(-i\varphi(r)\big)\big); \\ cos\,\theta\,(r)\,sin\,\theta\,(r)\big(1-exp\big(-i\varphi(r)\big)\big); & sin^2\,\theta\,(r)+cos^2\,\theta\,(r)\,exp\big(-i\varphi(r)\big) \end{bmatrix} \quad (1)$$

where θ is the direction of the optical axis; $\varphi=2\pi/\lambda\, l$– phase shift between orthogonal amplitude components; λ - wavelength; l - geometric path; Δn - birefringence index.

- The polarization properties of the external (rough) component of a histological section of a breast tumors biopsy are characterized by the Jones matrix of the following symmetry.

$$\{R\}=\begin{bmatrix} r_x/r_y & 0 \\ 0 & 1 \end{bmatrix} \quad (2)$$

Where r_x, r_y – Fresnel coefficients for orthogonal components of laser radiation amplitude.

- Superposition of matrix operators (1) and (2) defines total polarization manifestations of phase-inhomogeneous structure of layers of biological preparations.

$$\{F\}=\{K\}\{B\}=\begin{bmatrix} f_{11} & f_{12} \\ f_{21} & f_{22} \end{bmatrix}=\begin{bmatrix} (r_{11}b_{11}+r_{12}b_{21}) & (r_{11}b_{12}+r_{12}b_{22}) \\ (r_{21}b_{11}+r_{22}b_{21}) & (r_{21}b_{12}+r_{22}b_{22}) \end{bmatrix} \quad (3)$$

- Analytically, the complex amplitude formation scenario (H_x, H_y) of the object field of the breast tumour preparation layer is defined by the following Jones matrix equation.

$$(H)=\{F\}\big(H^{(0)}\big)\leftrightarrow\begin{pmatrix} H_x \\ H_y \end{pmatrix}=\begin{bmatrix} f_{11} & f_{12} \\ f_{21} & f_{22} \end{bmatrix}\begin{pmatrix} H_x^{(0)} \\ H_y^{(0)} \end{pmatrix} \quad (4)$$

where $\big(H^{(0)}\big)$ and (H) - the Jones vector of the illuminating and object laser beam;

$$\begin{pmatrix} H_x^{(0)} \\ H_y^{(0)} \end{pmatrix}=\begin{pmatrix} A_x^{(0)} \\ A_y^{(0)}\,exp\big(-i\varphi_{xy}^{(0)}\big) \end{pmatrix};\quad \begin{pmatrix} H_x \\ H_y \end{pmatrix}=\begin{pmatrix} A_x \\ A_y\,exp\big(-i\varphi_{xy}\big) \end{pmatrix};\quad \varphi_{xy}^{(0)}=\varphi_x^{(0)}-\varphi_y^{(0)};\quad \varphi_{xy}=\varphi_x-\varphi_y. \quad (5)$$

Here φ_{xy} -inter-amplitude phase shift.

- To describe the resulting structure of the object field of complex amplitudes, we used the traditional analytical operator - the coherence matrix $\{C\}$

$$\{C\}=\begin{bmatrix} c_{xx} & c_{xy} \\ c_{yx} & c_{yy} \end{bmatrix}=\begin{bmatrix} H_xH_x^* & H_xH_x^* \\ H_xH_x^* & H_yH_y^* \end{bmatrix}=\begin{bmatrix} (A_x)^2 & A_xA_y\,exp\big(-i\varphi_{xy}\big) \\ A_xA_y\,exp\big(i\delta_{xy}\big) & \big(A_y\big)^2 \end{bmatrix}. \quad (6)$$

Based on the operator $\{C(r)\}$, we characterize the degree of polarization $W(r)$ of the phase-inhomogeneous object field of the tumors preparation layer by the classical expression

$$W(r)=\sqrt{1-\frac{4\big|\big[\langle H_x(r,\tau)H_x^*(r,\tau)\rangle\langle H_y(r,\tau)H_y^*(r,\tau)\rangle-\langle H_x(r,\tau)H_y^*(r,\tau)\rangle\langle H_y(r,\tau)H_x^*(r,\tau)\rangle\big]\big|}{\big[\langle H_x(r,\tau)H_x^*(r,\tau)\rangle+\langle H_y(r,\tau)H_y^*(r,\tau)\rangle\big]^2}} \quad (7)$$

Here $\langle\ \rangle$ - means the time averaging operation.

Our proposed model analysis reveals ($\langle H\rangle=H$) and ($\langle\varphi_{xy}\rangle=\varphi_{xy}$) that for all points of scattered coherent radiation a 100% degree of polarization is formed

$$W(r)=\sqrt{1-\frac{4\big|\big[H_x(r)H_x^*(r)H_y(r)H_y^*(r)-H_x(r)H_y^*(r)H_y(r)H_x^*(r)\big]\big|}{\big[H_x(r)H_x^*(r)+H_y(r)H_y^*(r)\big]^2}}=1{,}0 \quad (8)$$

A solution to this problem can be a different analytical approach, which is based on the correlation ("two-point") method of describing the structure of scattered coherent radiation fields [24, 25].

This correlation approach uses an algorithm for determining the degree of coherence of complex amplitudes at different points of the scattered radiation field, which is called complex degree of coherence (CDC)

$$\omega(r_1, r_2) = \left[\frac{Tr(S^{\circ}(r_1,r_2)S(r_1,r_2))}{TrS(r_1,r_1)\cdot TrS(r_2,r_2)}\right] \quad (9)$$

Here $S(r_1,r_2)$ - transverse spectral density matrix

$$S(r_1, r_2) = \begin{bmatrix} H_x^*(r_1)H_x(r_2) & H_x^*(r_1)H_y(r_2) \\ H_y^*(r_1)H_x(r_2) & H_y^*(r_1)H_y(r_2) \end{bmatrix} \quad (10)$$

where $S(r_1, r_2)$ – hermitian conjugate matrix to matrix $S(r_1, r_2)$; Tr - matrix trace.

For our model representations of the optical structure of the skin, this approach allows expression (10) to be written as follows

$$S_{out}(r) = F^{\circ}(r) \cdot S_{in}(r) \cdot F(r). \quad (11)$$

Here $F(r)$ - Jones matrix histological section of a tumor of an analytical type (4); $F^{\circ}(r)$ - Hermitian conjugate operator; $S_{in}(r)$ - transverse spectral density matrix of the illuminating beam

$$S_{in}(r) = \begin{bmatrix} H_x^{(0)*}(r)H_x^{(0)}(r) & H_x^{(0)*}(r)H_y^{(0)}(r) \\ H_y^{(0)*}(r)H_x^{(0)}(r) & H_y^{(0)*}(r)H_y^{(0)}(r) \end{bmatrix} \quad (12)$$

Analysis of the complex expression (12) taking into account (1) - (3) and (10), (11) found that the modulus of the CDC $|\omega(r)|$ at each point of the object field is a constant value.

$$|\omega(r)| = W(r) = 1{,}0 \quad (13)$$

New diagnostic information about polarization-correlation manifestations of optically anisotropic skin properties can be provided by phase $\Delta(\mu(r)) \equiv \Delta(r)$, defined as

$$\Delta(r) = \frac{2A_x(r)A_y(r)\cos\varphi_{xy}(r)}{A_x^2(r)+A_y^2(r)} \quad (14)$$

The explicit form of the inter-amplitude phase shift $\varphi_{xy}(r)$ is determined from the matrix equation (4)

$$\varphi_{xy}(r) = arctg\left\{\frac{Im\left[f_{11}(r)H_x^{(0)}+f_{12}(r)H_y^{(0)}\right]}{Re\left[f_{11}(r)H_x^{(0)}+f_{12}(r)H_y^{(0)}\right]}\right\} - arctg\left\{\frac{Im\left[f_{21}(r)H_x^{(0)}+f_{22}(r)H_y^{(0)}\right]}{Re\left[f_{21}(r)H_x^{(0)}+f_{22}(r)H_y^{(0)}\right]}\right\} \quad (15)$$

Let's analyze (15) for a simple and often realized situation - probing a biological layer with a plane-polarized beam with azimuth 0^0 ($H_x^{(0)} \equiv 1{,}0; H_y^{(0)} = 0$)

$$\varphi_{xy}(r) = arctg\left\{\frac{Im(r_{11}b_{11})}{Re(r_{11}b_{11})}\right\} - arctg\left\{\frac{Im(b_{21})}{Re(b_{21})}\right\} = arctg\left\{\frac{Im(\cos^2\theta - \sin^2\theta\, exp(-i\varphi_x))}{Re(\cos^2\theta - \sin^2\theta\, exp(-i\varphi_x))}\right\} -$$
$$-arctg\left\{\frac{Im\left(\cos\theta\sin\theta(1-exp(-i\varphi_y))\right)}{Re\left(\cos\theta\sin\theta(1-exp(-i\varphi_y))\right)}\right\} = arctg\left\{\frac{\sin^2\theta\sin\varphi_x}{1-\sin^2\theta(1-\cos\varphi_x)}\right\} - arctg\left\{\frac{\sin\varphi_y}{1+\cos\varphi_y}\right\} \quad (16)$$

It can be shown that for $0 \le \varphi_{xy} \le \pi$ wide range of CDC phase change is realized.

$$0.0 \le \Delta(r) \le 1.0. \quad (17)$$

As a result of our analytical modeling, we determined a diagnostically sensitive polarization-correlation parameter for detecting changes in the structure of multiply scattered breast tumor preparations object fields of complex amplitudes.

5. Experimental Scheme and Methodology of Polarization Correlometry

Two groups of breast tumor specimens were studied:
- Group 1 - benign (fibroadenoma) tumors - 21 samples.

- Group 2 - malignant (sarcoma) - 19 samples. The objects of study were optically thick (geometric thickness $d = 55\mu m$, attenuation factor $\tau \leq 0{,}67$).

Histological sections of breast tumor biopsy, obtained according to the standard method on a freezing microtome.

Figure 1 illustrates the layout of a laser polarimeter for biological preparations, a detailed description of which can be found in [4-6].

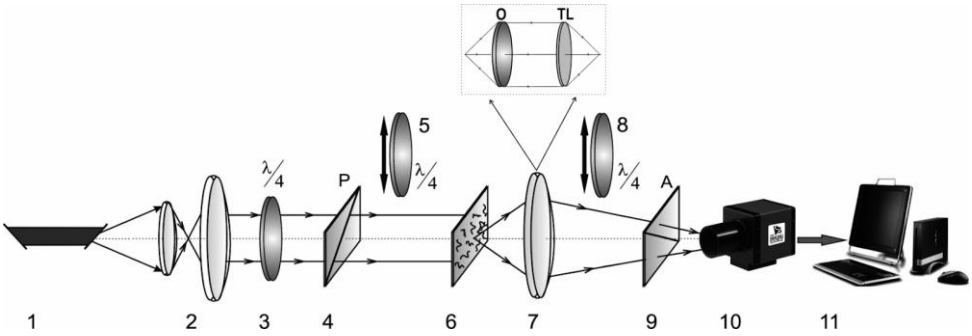

Fig. 1. Polarization correlometer:

1 - HeNe laser;
2 - optical collimator;
3, 5, 8 - phase-shifting elements;
4, 9 - linear polarizer and analyzer;
6 – biological sample;
7 - polarizing micro-lens (magnification x4);
10 - digital CCD camera;
11 - computer data processing unit.

The image of biological samples 6 was projected by a microlens 7 into the plane of the photosensitive area ($r \equiv m \times n = 800pix \times 600pix$) of the CCD camera 10.

We used the following mapping methodology of DLD:

- The transmission axis of the linear polarizer 9 is set in two discrete positions $\Omega = 0^0$, $\Omega = 90^0$, and the corresponding discrete $(m \times n)$ sets of intensity values $I_0\begin{pmatrix} r_{11} & \cdots & r_{1m} \\ \cdots & \cdots & \cdots \\ r_{n1} & \cdots & r_{nm} \end{pmatrix}$, $I_{90}\begin{pmatrix} r_{11} & \cdots & r_{1m} \\ \cdots & \cdots & \cdots \\ r_{n1} & \cdots & r_{nm} \end{pmatrix}$ are measured.
- The full range of polarizer transmission axis rotations is realized 9 ($\Theta = 0^0 \div 180^0$).
- For each discrete pixel the arrays of the maximum and minimum intensity levels $I\begin{pmatrix} r_{11} & \cdots & r_{1m} \\ \cdots & \cdots & \cdots \\ r_{n1} & \cdots & r_{nm} \end{pmatrix}_{min}$, $I\begin{pmatrix} r_{11} & \cdots & r_{1m} \\ \cdots & \cdots & \cdots \\ r_{n1} & \cdots & r_{nm} \end{pmatrix}_{max}$ and the values of the associated transmission axis rotation angles are measured $\Omega\begin{pmatrix} r_{11} & \cdots & r_{1m} \\ \cdots & \cdots & \cdots \\ r_{n1} & \cdots & r_{nm} \end{pmatrix}\left(I\begin{pmatrix} r_{11} & \cdots & r_{1m} \\ \cdots & \cdots & \cdots \\ r_{n1} & \cdots & r_{nm} \end{pmatrix} \equiv I_{min}\right)$.
- Algorithmically calculated maps of the azimuth and ellipticity

$$\alpha\begin{pmatrix} r_{11} & \cdots & r_{1m} \\ \cdots & \cdots & \cdots \\ r_{n1} & \cdots & r_{nm} \end{pmatrix} = \Omega\left(I(r)_{min}\frac{\pi}{2}\right)$$
$$\beta\begin{pmatrix} r_{11} & \cdots & r_{1m} \\ \cdots & \cdots & \cdots \\ r_{n1} & \cdots & r_{nm} \end{pmatrix} = arctg\,\frac{I(r)_{min}}{I(r)_{max}}. \quad (18)$$

- Calculate the phase map of the scattered radiation $\varphi\begin{pmatrix} r_{11} & \cdots & r_{1m} \\ \cdots & \cdots & \cdots \\ r_{n1} & \cdots & r_{nm} \end{pmatrix}$

$$\varphi(r) = arctg\left[\frac{tg2\beta(r)}{tg\alpha(r)}\right] \quad (19)$$

- Calculate the map DLD $\Delta\begin{pmatrix} r_{11} & \cdots & r_{1m} \\ \cdots & \cdots & \cdots \\ r_{n1} & \cdots & r_{nm} \end{pmatrix}$

$$\Delta(r) = arctg\frac{I_0^{0,5}(r)I_{90}^{0,5}(r)\cos\varphi(r)}{I_0(r)+I_{90}(r)} \quad (20)$$

6. Analytical Approaches to Polarization-Correlation Data Processing

The single-point methods of imaging polarimetry, in the vast majority of cases, rely on statistical analysis of the obtained data and are somewhat information-limited. They do not provide any information about the topographical structure of the polarization images of biological layers, as well as their scale-invariant self-similarity. Moreover, algorithms for correlation and fractal analysis are rarely used for the objective assessment of such "unexplored" structures in laser images. Therefore, in our work, we employed a comprehensive and comparative analysis that enables us to obtain information about both statistical and topographical aspects, as well as the scale-invariant self-similar structure of polarization-correlation maps.

We applied three methods for analytical treatment of two-dimensional arrays $\Delta(x = 1 \div m; y = 1 \div n)$ [5 - 2].

Statistical approach:

$$R_1^{\Delta} = \frac{1}{M}\sum_{i=1}^{M}|\Delta_i|,\ R_2^{\Delta} = \sqrt{\frac{1}{M}\sum_{i=1}^{M}\Delta_i^2},\ R_3^{\Delta} = \frac{1}{\left(R_2^{\Delta}\right)^3}\frac{1}{M}\sum_{i=1}^{M}\Delta_i^3,\ R_4^{\Delta} = \frac{1}{\left(R_2^{\Delta}\right)^2}\frac{1}{M}\sum_{i=1}^{M}\Delta_i^4 \quad (21)$$

Here $R_{j=1,2,3,4}^{\Delta}$ – central Δstatistical moments that characterize the mean, variance, skewness and kurtosis of the distribution Δ(x=1÷m; y=1÷n), M - digital camera pixel count.

Correlation approach:

$$A_{i=1\div n}^{\Delta}(\Delta m) = \lim_{m\to 0}\frac{1}{m}\int_1^m[\Delta(m)][\Delta(m-\Delta m)]dm \quad (22)$$

Here $A_{i=1\div n}^{\Delta}(\Delta m)$ – autocorrelation function, $\Delta m = 1pix$.

The final average over all lines of the digital polarization-correlation map is the following expression.

$$A^{\Delta}(\Delta m) = \frac{\sum_{i=1}^{n}A_i^{\Delta}(\Delta m)}{n} \quad (23)$$

To quantify the autocorrelation dependences $A^{\Delta}(\Delta m)$, we chose:

- "correlation area" S^{μ}

$$S^{\Delta} = \int_1^m A^{\Delta}(\Delta m)dm \quad (24)$$

The fractal approach: The fractal analysis of distributions $\Delta(m \times n)$ was based on the calculation of the logarithmic dependences $log\,J\,(\Delta) - log\,d^{-1}$ of the power spectra $J(\Delta)$

$$J(\mu) = \int_{-\infty}^{+\infty}\Delta\cos 2\pi\nu d\nu \quad (25)$$

where $\nu = z$ is the spatial frequencies of the of the objective field of a blood serum sample.

For the dependences $log\,J\,(\Delta) - log\,d^{-1}$ the slope angle η of the approximating curves $V(\eta)$ was determined and the fractal dimensions were calculated.

$$F^{\Delta} = 3 - tg\eta. \quad (26)$$

Classification of coordinate distributions $\Delta(x \times y)$ was carried out according to the following criteria:

- $\Delta(x \times y)$ – fractal or self - similar in the presence of a constant angle $\eta = const$ of inclination within 2 - 3 decades of size changes d ;
- $\Delta(x \times y)$ – multifractal in the presence of several angles of inclination $V(\eta)$;
- $\Delta(x \times y)$ – random in the absence of stable angles of inclination $V(\eta)$ in the entire range of resizing d.

All distributions $log\,J\,(\Delta) - log\,d^{-1}$ were characterized by dispersion.

$$D^{\Delta} = \sqrt{\frac{1}{N}\sum_{i=1}^{N}[log\,J\,(\Delta) - log\,d^{-1}]_i^2} \quad (27)$$

7. Information Analysis

To determine the clinical applicability of the algorithmic information (the relationships (21)-(27)), we employed an information analysis of the results of polarization-correlation mapping using a set of operational characteristics of evidence-based medicine [25]:

- Sensitivity (Se) - the proportion of true positive results (A) of the diagnostic method among all samples from the experimental group 2 (N)

$$Se = \frac{A}{N}100\%. \tag{28}$$

- Specificity (Sp) is the proportion of true negative results (B) of the method among all samples from the control group 1 (H).

$$Sp = \frac{B}{H}100\%. \tag{29}$$

- Accuracy (Ac) is the proportion of correct results (A+B) of the test among all samples (N+H)

$$Ac = \frac{A+B}{N+H}100\%. \tag{30}$$

If N+H, it is called balanced accuracy Ac.

8. Experimental Results and Discussion

Figure 2 illustrates polarization-visualized in the crossed axes of polarizer 4 and analyzer 9 microscopic images of histological sections of biopsied benign fibroadenoma (fragment (a)) and sarcoma (fragment (b)) of the breast.

(a) (b)

Fig. 2. Polarization-visualized in crossed axes of polarizer 4 and analyzer 9 microscopic images of histological sections of biopsies of benign fibroadenoma (fragment (a)) and sarcoma (fragment (b)) of the breast.

The results of direct polarization photography of histological sections of breast tumor biopsy specimens indicate the presence of a volumetric optically anisotropic component, the properties of which are characterized by relations (1)-(8). Experimentally, this manifests itself as ensembles of domains of different shapes and intensities. At the same time, there are no obvious (visual) differences between the scattered object fields of histological sections of fibroadenoma (Fig. 2, fragment (a)) and sarcoma (Fig. 2, fragment (b)).

Results of polarization-correlation mapping of parameter distributions (relation (19)) DLD $\Delta(x \times y)$ of object fields of samples of both types are presented in the series of fragments (a) and (b) of Fig. 3.

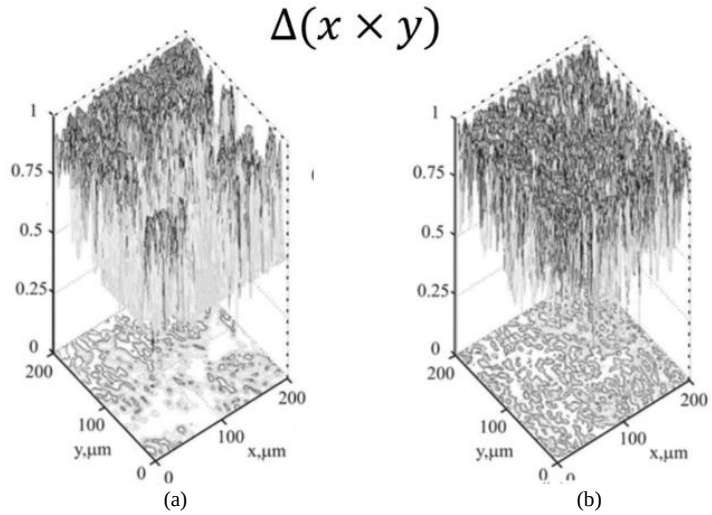

Fig. 3. Scatterplot maps Δ(x × y) of histological sections of fibroadenoma (a) and sarcoma (b).

As can be seen, the experimentally measured polarization-correlation maps $\Delta(x \times y)$ of both types of samples are characterized by the widest possible range of variation of the eigenvalues $0 \leq \Delta(x \times y) \leq 1$. In addition, the $\Delta(x \times y)$) distributions have a complex coordinate-heterogeneous topological structure of local domains of different shape and scale.

From a physical point of view, the obtained results can be explained by the complex spatial-angular structure of birefringent fibrous protein networks within the volume of histological sections of breast tissue biopsies. In each point of such samples, individual values of the optical axis direction of the biological crystal and the phase shift it introduces between the orthogonal components of laser radiation amplitude (equations (1)-(5)) are realized. As a result, a random, generally elliptical, polarization type is formed (equation (6)). For the set of all points in such polarizationally inhomogeneous images, there arises a coordinate inhomogeneity of their polarization-correlation alignment (equations (7)-(13)), which is characterized by a wide range of variation in the phase of local degree of depolarization (equations (14)-(17)).

Based on this, we carried out a comprehensive statistical, correlation, and fractal analysis of various discrete samples of $\Delta(x \times y)$ polarization-correlation map values:

- "minimal" ($\Delta_{min} = 0$) – object field areas formed by optically isotropic domains of histological sections of breast tumors, for which phase shifts $\sigma = 0rad$;
- "average" ($\tilde{\Delta} = 0{,}45$) - object field areas formed by optically anisotropic domains of histological sections of breast tumors for which the phase shift value reaches $\sigma = 0.3\pi$.
- "maximum" ($\Delta_{max} = 1$), which correspond to extreme phase shifts ($\sigma = 0.5\pi$).

By means of a horizontal scan (step $\Delta x = 1pix$) of the $\Delta(x \times y)$ distribution columns, the distributions of the number of digital samples indicated were calculated:

- $Q_{min}(x) \equiv ({Q_{min}}^{(1)}, \ {Q_{min}}^{(2)}, \ \ldots, \ {Q_{min}}^{(m)})$;
- $Q(x) \equiv (\tilde{Q}^{(1)}, \ \tilde{Q}^{(2)}, \ \ldots, \ \tilde{Q}^{(m)})$;
- $Q_{max}(x) \equiv ({Q_{max}}^{(1)}, \ {Q_{max}}^{(2)}, \ \ldots, \ {Q_{max}}^{(m)}$.

The resulting dependencies were processed using complex statistical, autocorrelation and scale-sample analysis for both types of breast tumor samples - Fig. 4 - Fig. 6.

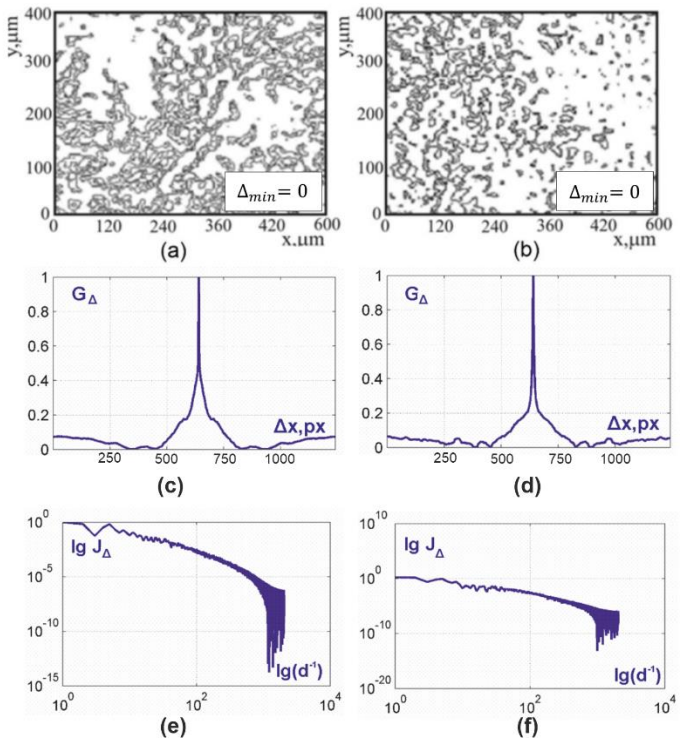

Fig. 4. Discrete sampling maps $\Delta_{min}= 0$ ((a), (b)), autocorrelation functions ((c), (d)) and scale-sample relationships ((e), (f)) for histological sections of fibroadenoma biopsies ((a), (c), (e)) and sarcoma ((b), (d), (f)) in breast.

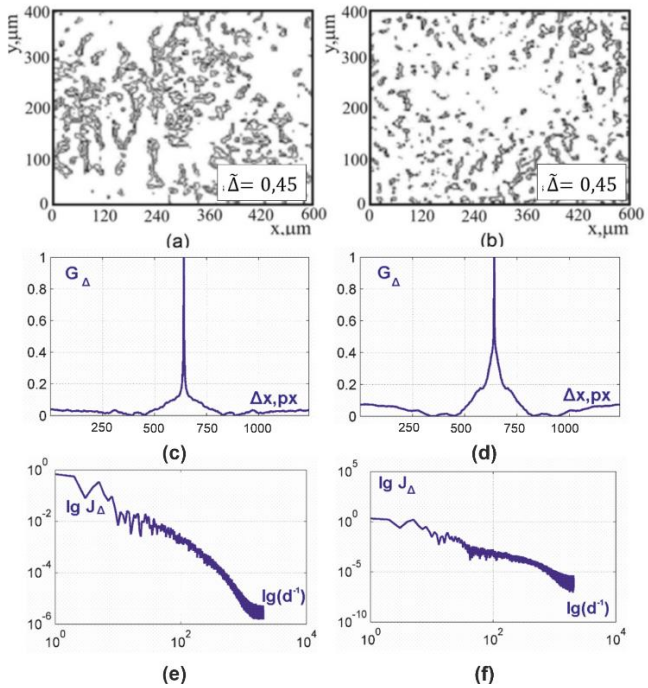

Fig. 5. Discrete sampling maps $\tilde{\Delta}= 0{,}45$ (a), (b)), autocorrelation functions ((c), (d)) and scale-sample relationships ((e), (f)) for histological sections of fibroadenoma ((a) , (c), (e)) and sarcoma ((b), (d), (f)) breast biopsies.

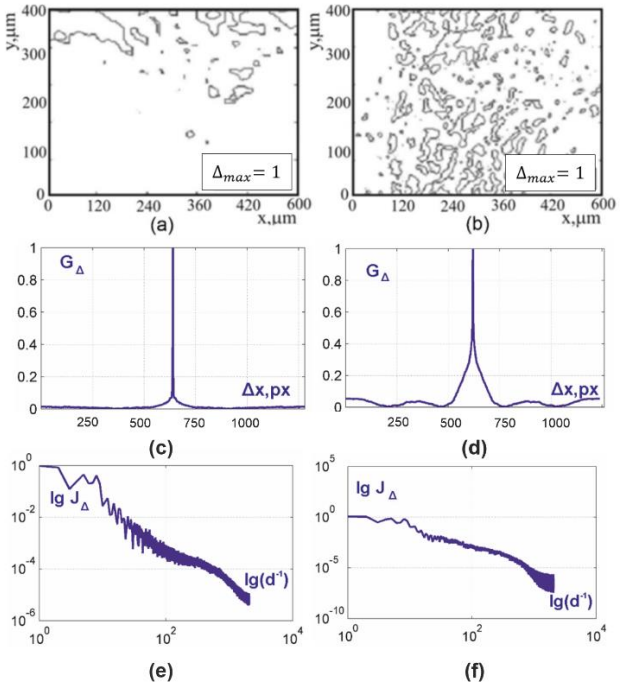

Fig. 6. Discrete sampling maps $\Delta_{max}= 1$ ((a), (b)), autocorrelation functions ((c), (d)) and scale-sample relationships ((e), (f)) for histological sections of fibroadenoma ((a) , (c), (e)) and sarcoma ((b), (d), (f)) breast biopsies.

Comparison of the experimental data set (Fig. 3 to Fig. 5) revealed:

- an increase in the number of sample values $\Delta_{min}= 0$ in the objective field of breast sarcoma biopsy histology specimens (Fig. 3 - Fig. 5, fragments (a) and (b));
- predominant decrease in the magnitude of correlation area of autocorrelation functions of local depolarization maps for fibroadenoma biopsy specimens in comparison with analogous relations obtained for breast sarcoma specimens (Fig. 3 - Fig. 5, fragments (c) and (d));
- the trend of destruction of mass self-similarity of discrete sampling maps of the degree of local depolarization of fibroadenoma biopsy histology specimens (Fig. 3 - Fig. 5, fragments (e), (f)).

Biophysically, these trends can be explained by an increase in birefringence of newly formed fibrillary protein networks of breast carcinoma. As a result, polarization heterogeneity of object fields of such samples increases, which is manifested by an increase in formation probability $\Delta(x \times y) = 0$ (relations (13) - (17)) and corresponding changes in the set of objective statistical, correlation and fractal parameters.

Quantitative dependences $Q(x)_{min}$, $\tilde{Q}(x)$, $Q(x)_{max}$, characterize statistical $R^{\Delta}_{i=1-4}$, correlation $S^{\Delta}$and fractal F^{Δ}, D^{Δ}, parameters determined within two groups of samples benign and malignant breast tumors - table 1.

Table 1. Objective parameters of the distributions of discrete local depolarization degree values of benign and malignant breast tumor samples

$Q(x)$	$Q(x)_{max}$		$\tilde{Q}(x)$		$Q(x)_{min}$	
	fibroadenoma ($q = 21$)	sarcoma ($q = 19$)	fibroadenoma ($q = 21$)	sarcoma ($q = 19$)	fibroadenoma ($q = 21$)	sarcoma ($q = 19$)
R^{Δ}_1	0.45±0.053	0.43±0.02	0.33±0.024	0.44±0.025	0.07±0.00	0.22±0.015
R^{Δ}_2	0.13±0.011	0.14±0.009	0.15±0.013	0.16±0.008	0.42±0.021	0.16±0.009
R^{Δ}_3	0.22±0.024	0.31±0.018	0.56±0.07	0.43±0.035	1.61±0.17	0.71±0.041
R^{Δ}_4	0.44±0.053	0.52±0.047	0.73±0.061	0.61±0.072	2.15±0.12	0.84±0.01
S^{Δ}	0.23±0.013	0.24±0.011	0.15±0.013	0.07±0.004	0.13±0.003	0.04±0.002
D^{Δ}	0.15±0.024	0.18±0.008	0.31±0.024	0.14±0.015	0.43±0.027	0.23±0.025
F^{Δ}	1.91±0.026	1.91±0.017	2.11±0.015	2.11±0.011	-	2.28±0.021

The following markers have been found to be diagnostically sensitive for breast sarcoma:

- Mean, variance, skewness and kurtosis, which characterize $Q(x)$ distributions - the differences between them are 2 - 3 times;
- 2 to 5 times increase in the correlation area S^{Δ} of autocorrelation functions $\tilde{A}(\Delta x)$ and $A(\Delta x)_{min}$;
- destruction of scale self-similarity of discrete sampling distributions $N(x)_{min}$for fibroadenoma object fields;

- 2 times increase in the value of D^{Δ} which characterizes the logarithmic $log\, J\,(Q_{min} - log\, d^{-1})$ dependencies of the carcinoma object field samples.

The results of the information analysis regarding the determination of the clinical effectiveness of the proposed method of polarization-correlation mapping of histological sections from benign and malignant breast tumors are presented in Table 2.

Table 2. Accuracy of the differential diagnosis of polarization-correlation mapping of images of benign and malignant breast tumor samples.

Parameters	R_1^{Δ}	R_2^{Δ}	R_3^{Δ}	R_4^{Δ}	S^{Δ}	T^{Δ}	F^{Δ}	D^{Δ}
Accuracy, %	87	85	92	94	92	96	86	90

The data analysis from polarization-correlation mapping determined the following accuracy levels for the differential diagnosis of breast cancer using different markers:

- Statistical analysis - very good accuracy $Ac(R_4^{\Delta}) = 94\%$;
- Correlation analysis - excellent accuracy $Ac(T^{\Delta}) = 96\%$;
- Fractal analysis - good accuracy $Ac(D^{V}) = 90\%$.

However, these are only initial results from the clinical evaluation of the polarization-correlation mapping method. Ahead lies extensive systematic work for the large-scale implementation of the developed technique, taking into account the influence of numerous demographic, societal, social, and other factors on its reproducibility, accuracy, and clinical effectiveness.

9. Conclusions

A new analytical algorithm for describing the structure of multiply scattered by biological tissues polarization-inhomogeneous laser fields using an original parameter - the degree of local depolarization - is proposed.

A method for measuring coordinate distributions of the degree of local depolarization has been developed and experimentally tested.

Diagnostic sensitivity of algorithms of statistical, autocorrelation and scale-similar analysis of discrete samples of local depolarization degree distributions in differentiation of benign fibroadenoma and malignant breast sarcoma was demonstrated.

The proposed methodology extends the functional capabilities of traditional histological examinations of breast tumor biopsies and enables rapid and objective detection of cancer development.

Acknowledgments

This work received funding from: National Research Foundation of Ukraine, Project 2020.02/0061; Project 2022.01/0034 and Scholarship of the Supreme Council for Young Scientists - Doctor of Sciences.

Conflict of Interest

The authors declare no competing interests.

Ethics Approval and Consent to Participate

This study was conducted in accordance with the principles of the Declaration of Helsinki, and in compliance with the International Conference on Harmonization-Good Clinical Practice and local regulatory requirements. Ethical approval was obtained from the Ethics Committee of the Bureau of Forensic Medicine of the Chernivtsi National University and the Bukovinian State Medical University (Chernivtsi, Ukraine), and written informed consent was obtained from all subjects prior to study initiation.

References

[1] S. Mallat, "A theory for multiresolution signal decomposition: the wavelet representation," IEEE Trans. Pattern Anal. Mach. Intell. 11(7), 674–693 (1989).

[2] Ghosh, N. Tissue polarimetry: concepts, challenges, applications, and outlook. J. Biomed. Opt. 16, 110801 (2011).

[3] Jacques, S. L. Polarized light imaging of biological tissues. in Handbook of Biomedical Optics2 (eds. Boas, D., Pitris, C. & Ramanujam, N.) 649–669 (CRC Press, 2011).
[4] Vitkin, A., Ghosh, N. & de Martino, A. Tissue Polarimetry. in Photonics: Scientific Foundations, Technology and Applications (ed. Andrews, D. L.) 239–321 (John Wiley & Sons, Ltd, 2015).
[5] P O Angelsky, A G Ushenko, etc. The singular approach for processing polarization-inhomogeneous laser images of blood plasma layers, Journal of Optics, 2013, Volume 15, Number 4.
[6] Vasyl P Pishak, Alexander G Ushenko, etc. "Polarization structure of biospeckle fields in crosslinked tissues of a human organism: 1. Vector structure of skin biospeckles", Proceedings Volume 3317, International Conference on Correlation Optics; (1997) https://doi.org/10.1117/12.295715.
[7] Volodimir Ushenko, Anton Sdobnov, Anna Syvokorovskaya, et.al. 3D Mueller-Matrix Diffusive Tomography of Polycrystalline Blood Films for Cancer Diagnosis//Photonics 2018, 5(4), 54.
[8] N. I. Zabolotna, S. V. Pavlov, etc. "System of the phase tomography of optically anisotropic polycrystalline films of biological fluids," Proceedings Volume 9166, Biosensing and Nanomedicine VII, 916616 (2014).
[9] O. G Ushenko, A. V. Dubolazov, etc. "Wavelet analysis for polarization inhomogeneous laser images of blood plasma", Proceedings Volume 8338, Tenth International Conference on Correlation Optics; 83381H (2011).
[10] Romuald Jóźwicki, Krzysztof Patorski et.al. Automatic polarimetric system for early medical diagnosis by biotissue testing Optica Applicata, Vol. XXXII, No. 4, 2002.
[11] Motahareh Peyvasteh, Liliya Tryfonyuk, etc. "3D Mueller-matrix-based azimuthal invariant tomography of polycrystalline structure within benign and malignant soft-tissue tumours", 2020, Laser Physics Letters, 17 (11), 115606.
[12] Hassan, D. K., Suhaimi, H., Bilad, M. R., & Abas, P. E. (2023). Automated Cell Counting using Image Processing. International Journal of Computing, 22(3), 302-310.
[13] Anton Sdobnov, Volodymir A. Ushenko, etc. Mueller-matrix imaging polarimetry elevated by wavelet decomposition and polarization-singular processing for analysis of specific cancerous tissue pathology, J. Biomed. Opt. 28(10), 102903 (2023), doi: 10.1117/1.JBO.28.10.102903.
[14] Atam Kumar, Hafiz Karim Bux Indher, Ali Gul, Rab Nawaz, "Analysis of Risk Factors for Work-related Musculoskeletal Disorders: A Survey Research", International Journal of Engineering and Manufacturing, Vol.12, No.6, pp. 1-13, 2022.
[15] Ushenko, V.A., Hogan, B.T., etc. "3D Mueller matrix mapping of layered distributions of depolarisation degree for analysis of prostate adenoma and carcinoma diffuse tissues", 2021, Scientific Reports, 11 (1), 5162.
[16] Y. Meyer, Wavelets: Algorithms and Applications, Society for Industrial and Applied Mathematics (SIAM), Philadelphia (1993).
[17] Trifonyuk, L., Sdobnov, A., etc. "Differential Mueller matrix imaging of partially depolarizing optically anisotropic biological tissues", 2020, Lasers in Medical Science, 35 (4), pp. 877-891.
[18] Chakre, R. R., & Patil, D. V. (2023). Classification of Brain Tumor using Dendritic Cell-Squirrel Search Algorithm in a Parallel Environment. International Journal of Computing, 22(3), 389-396. https://doi.org/10.47839/ijc.22.3.3235.
[19] Farzin Salmasi, Mohammad Taghi Sattari, Halit Apaydin, " Mathematical Based Implicit and Explicit Finite Difference Techniques for Solving the Ground Water Flow Equations Using Spreadsheets", International Journal of Mathematical Sciences and Computing, Vol.8, No.4, pp. 1-14, 2022.
[20] Borovkova, M., Trifonyuk, L., etc. "Mueller-matrix-based polarization imaging and quantitative assessment of optically anisotropic polycrystalline networks", 2019, PLoS ONE, 14 (5), e0214494.
[21] Gholam Reza Moghissi, Ali Payandeh, "Revised Method for Sampling Coefficient Vector of GNR-enumeration Solution", International Journal of Mathematical Sciences and Computing, Vol.8, No.3, pp. 1-20, 2022.
[22] Borovkova, M., Peyvasteh, M., etc. "Complementary analysis of Mueller-matrix images of optically anisotropic highly scattering biological tissues", 2018, Journal of the European Optical Society, 14 (1), 20.
[23] Ushenko, V.A., Sdobnov, A.Y., etc. "Biomedical applications of Jones-matrix tomography to polycrystalline films of biological fluids", 2019, Journal of Innovative Optical Health Sciences, 12 (6), 1950017.
[24] Beam coherence polarization matrix / F. Gori, M. Santarsiero, S. Vicalvi, R. Borghi, G. Guattari // Pure Appl. Opt. – 1998. – Vol. 7. – P. 941-951.
[25] J. Tervo, T. Setala, A. Friberg, "Two-point Stokes parameters: interpretation and properties," Optics Letters 34(20), 3074 - 3076 (2009).

Authors' Profiles

Yuriy Ushenko was born on December 23, 1980, in Chishinau, Moldova. M.Sc. in Telecommunications (2003). PhD in Optics and Laser Physics (2006). D.Sc. in Optics and Laser Physics, Taras Shevchenko National University of Kyiv (2015). Current position – Professor, Head of Computer Science Department, Chernivtsi National University, Ukraine. Research Interests: Data Mining and Analysis, Computer Vision and Pattern Recognition, Optics & Photonics, Biophysics.

Valentina Dvorzhak was born on September 27, 1982, in Kramatorsk, Ukraine. M.Sc. in Metallurgical Engineering (2004). Ph.D. in Technical Science, Donbass State Engineering Academy (2007). Current position – Assistant Professor of Computer science department, Chernivtsi National University, Ukraine. Research Interests: Data Mining and Analysis, Computer Vision and Pattern Recognition, Optics & Photonics, Biophysics, Metal Forming Technology & Equipment.

Oleksandr Dubolazov, Associate Professor at the Chernivtsi National University. He received his BS and MS degrees in optics from the Chernivtsi National University in 2006 and 2007, respectively, and his PhD degree in optics, laser physics from the Chernivtsi National University in 2010. He is the author of more than 100 journal papers and has written five book chapters. His current research interests include laser polarimetry, holography etc.

Oleksandr Ushenko, Professor at Chernivtsi National University, Head of Optics and Publishing Department. He received his BS and MS degrees in Optics from the Chernivtsi State University in 1975 and 1977, respectively, and his PhD degree in Optics and Laser Physics from the Chernivtsi State University in 1983. In 2000 he obtained D.Sc. in Optics and Laser Physics. He is the author of more than 200 journal papers, 60 patents and 20 monographies. His current research interests include laser polarimetry, polarization interferometry and digital holography.

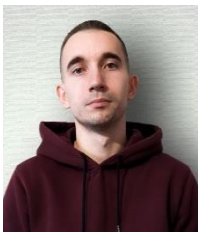

Ivan Mikirin, Postgraduate student at the Optics and Publishing Department of Chernivtsi National University. Research interests - digital processing of medical images using computer algorithms of statistical, correlation and fractal analysis.

Zhengbing Hu, Prof., Deputy Director, International Center of Informatics and Computer Science, Faculty of Applied Mathematics, National Technical University of Ukraine "Kyiv Polytechnic Institute", Ukraine. Adjunct Professor, School of Computer Science, Hubei University of Technology, China. Visiting Prof., DSc Candidate in National Aviation University (Ukraine) from 2019. Major research interests: Computer Science and Technology Applications, Artificial Intelligence, Network Security, Communications, Data Processing, Cloud Computing, Education Technology.

How to cite this paper: Yuriy Ushenko, Valentina Dvorzhak, Oleksandr Dubolazov, Oleksandr Ushenko, Ivan Mikirin, Zhengbing Hu, "Analytical and Computer Polarization-Correlation Processing of Brest Tumors' Laser Fields for Cancer Detection", International Journal of Image, Graphics and Signal Processing(IJIGSP), Vol.15, No.6, pp. 41-53, 2023. DOI:10.5815/ijigsp.2023.06.04